

Low-Frequency Earthquakes and Pore Pressure Transients in Subduction Zones

Nikolaï Shapiro, Michel Campillo, Edouard Kaminski, Jean-pierre Vilotte, Claude Jaupart

▶ **To cite this version:**

Nikolaï Shapiro, Michel Campillo, Edouard Kaminski, Jean-pierre Vilotte, Claude Jaupart. Low-Frequency Earthquakes and Pore Pressure Transients in Subduction Zones. Geophysical Research Letters, 2018, 45 (20), pp.11,083-11,094. 10.1029/2018GL079893 . insu-02927284

HAL Id: insu-02927284
https://insu.hal.science/insu-02927284

Submitted on 1 Sep 2020

HAL is a multi-disciplinary open access archive for the deposit and dissemination of scientific research documents, whether they are published or not. The documents may come from teaching and research institutions in France or abroad, or from public or private research centers.

L'archive ouverte pluridisciplinaire **HAL**, est destinée au dépôt et à la diffusion de documents scientifiques de niveau recherche, publiés ou non, émanant des établissements d'enseignement et de recherche français ou étrangers, des laboratoires publics ou privés.

Geophysical Research Letters

RESEARCH LETTER
10.1029/2018GL079893

Key Points:
- Radiation of low-frequency earthquakes can be explained by a single-force mechanism
- Rapid fluid pressure changes occur within the fault zone
- The fluid flux is provided by slab dehydration

Correspondence to:
N. M. Shapiro,
nshapiro@ipgp.fr

Citation:
Shapiro, N. M., Campillo, M., Kaminski, E., Vilotte, J.-P., & Jaupart, C. (2018). Low-frequency earthquakes and pore pressure transients in subduction zones. *Geophysical Research Letters*, *45*. https://doi.org/10.1029/2018GL079893

Received 6 AUG 2018
Accepted 9 OCT 2018
Accepted article online 12 OCT 2018

©2018. American Geophysical Union. All Rights Reserved.

Low-Frequency Earthquakes and Pore Pressure Transients in Subduction Zones

Nikolai M. Shapiro[1,2], Michel Campillo[3], Edouard Kaminski[1], Jean-Pierre Vilotte[1], and Claude Jaupart[1]

[1]Institut de Physique du Globe de Paris, Univ. Paris Diderot, Paris, France, [2]Schmidt Institute of Physics of the Earth, Russian Academy of Sciences, Moscow, Russia, [3]Institut des Sciences de la Terre, Université Grenoble Alpes, Grenoble Cedex, France

Abstract Low-frequency earthquakes (LFEs) have been observed in subduction zones and some major tectonic faults and may well be the most important constituents of tectonic tremors. In subduction zones, they were initially attributed to fluids released by dehydration reactions in downgoing slabs. Their seismic radiation pattern, however, is consistent with shear slip on the subduction interface, and this rapidly became the favored model. Recent studies indicate that the source duration of LFEs does not scale with magnitude, which can hardly be explained by shear rupture. We revisit the characteristics of LFE events in subduction zones as retrieved from local seismic arrays. We demonstrate that they can be explained equally well by forces acting in the direction of fluid motion. Such forces may be generated by a fast local pressure variations associated with unsteady fluid motion. The amount of fluid required for LFE activity is consistent with dehydration reaction rates.

Plain Language Summary We discuss possible mechanisms of the low-frequency earthquakes, a component of the slow earthquake phenomena observed in fault zones, and suggest that they can be generated by very rapid fluid transients releasing the strong pressures gradients built during nonstationary fluid transport in the fault zones.

1. Introduction

Since their discovery in Japan by Obara (2002), tectonic tremors have been observed in many subduction and fault zones (e.g., Husker et al., 2012; Kao et al., 2005; Kostoglodov et al., 2010; Nadeau & Dolenc, 2005; Payero et al., 2008; Walter et al., 2011). Drawing on analogies with volcanic tremors (e.g., Chouet, 1996; Fehler, 1983), early authors attributed them to fluid-driven seismogenic processes and named them "nonvolcanic tremors." More detailed observations have motivated other hypotheses. First, it was established that, in subduction zones, these tremors are closely associated with slow slip events (e.g., Obara & Hirose, 2006; Rogers & Dragert, 2003; Schwartz & Rokosky, 2007). They are in large part composed of low-frequency earthquakes (LFEs) characterized by small coherent impulsive arrivals recorded at several stations (Shelly et al., 2006). LFE hypocenters are aligned with the subduction interface and their radiation patterns can be explained by shear slip along that interface (e.g., Bostock et al., 2012; Frank et al., 2013; Ide et al., 2007; Shelly et al., 2007). This has led to models that consider slow slip events, tremors and LFEs as part of the same "slow earthquake" process, such that LFEs and tremors are generated by small stick-slip asperities in a larger slowly sliding fault.

The stick-slip asperity model is attractive but does not account for several observations. LFEs occur as clusters of many hundreds or thousands of highly repetitive multiplets, implying that their sources are very close to one another and are due to the same physical mechanism. According to recent studies, LFE source duration scales poorly with magnitude (e.g., Bostock et al., 2015; Farge et al., 2017), casting doubt on the validity of the self-similar rupture model that has been so successful for "regular" earthquakes. The nearly constant source duration of LFEs implies the predominance of asperities that have a well-defined characteristic size and yet slip by variable amounts. Processes that could account for a nearly constant asperity size have not been identified, however. We shall show that several LFE features, such as their radiation pattern, may be explained by mechanisms other than shear slip.

In this paper, we reexamine the possibility that LFEs are related to fluid transients in subduction zones. Our study is motivated by analogies between tectonic LFEs and volcanic long-period earthquakes, and

particularly those that occur at similar depths in subduction zones and active volcanic areas (Shapiro et al., 2017). We first show that the LFE seismic radiation pattern observed over a local seismic array can be explained by a single force mechanism as well as by a double-couple one. We propose that such forces arise from rapid pressure perturbations generated by fluid flow transients along the subduction interface. Finally, we estimate the amounts of fluids required to generate the observed LFE activity and find that they are consistent with petrologically-derived values for dehydration reactions in downgoing slabs (e.g., van Keken et al., 2011).

2. The Radiation Pattern of LFEs

Determining LFE focal mechanisms in subduction zones is fraught with many difficulties because radiation patterns must be extracted out of low signal-to-noise and relatively high-frequency waveforms. Ide et al. (2007) compared stacked LFE waveforms in Shikoku, Japan, to those of earthquakes with known mechanisms in the neighbouring subducting Philippine Sea Plate. They derived focal mechanisms from *P* wave polarities and moment tensors from *S* waveforms and concluded that both characteristics are consistent with shear slip on the plate interface. A similar approach was applied to LFEs in Cascadia and Mexico by Bostock et al. (2012), Royer and Bostock (2014), and Frank et al. (2013). In another approach the polarization of tectonic tremors has been measured and found approximately parallel to the direction of relative plate motion, which is consistent with *S* waves generated by the shear slip on the plate interface (e.g., Wech & Creager, 2007; Imanishi et al., 2016). These observations have provided strong support for a shear-slip origin for LFEs and tectonic tremors (Shelly et al., 2007).

The weak LFE signals are recorded in local seismic arrays directly above source regions. In subduction zones with relatively gently dipping slabs, these arrays are located in the vicinity of the *P* wave nodal planes of potential pure shear slip events. The *P* wave radiation pattern of a pure shear slip event is mainly controlled by the $\sin(2\theta)$ term, where θ is the angle with respect to the nodal plane (Aki & Richards, 2002). For a single impulsive force acting in the shear direction, the radiation pattern is $\propto \sin(\theta)$ instead, but this is almost identical to the previous one over the limited aperture of a local seismic array, as illustrated in Figure 1a. In such an array, *S* waves are mainly observed in transverse motion components with radiation patterns $\propto \cos(2\theta)$ and $\cos(\theta)$ for shear slip and single force events, respectively, which are again very close to each other for small θ values. *S* wave radiation patterns are distinctive at angles θ close to 45°, where *S* nodal planes are expected for shear slip mechanisms (Figure 1b). LFE recordings are rare at such high angles, however, and those that are available are plagued by lower signal to noise ratios due to larger source-to-receiver distances. *S* wave polarisation direction from a single force mechanism is parallel to the force vector. In a case of upward fluid motion along the plate interface, this force would be nearly parallel to the inter-plate slip vector. In such configuration, at stations just above the source a double couple and a single force mechanisms will generate *S* waves with nearly parallel polarization directions and, therefore, cannot be distinguished base on simple polarization analysis of tremors. Thus, the very configuration of local seismic arrays in subduction zones does not allow discrimination between shear slip and single force mechanisms.

We therefore conclude that the radiation pattern of subduction zone LFEs may well be due to a single impulsive force and look for potential physical mechanisms. Single-force mechanisms are generated by volcanic blasts and landslides (e.g., Dahlen, 1993; Ekström et al., 2003; Favreau et al., 2010; Kanamori & Given, 1982; Kanamori et al., 1984; Kawakatsu, 1989). They can also result from deep mass transport processes (Takei & Kumazawa, 1994), for example, in active volcanic conduits (e.g., Chouet & Matoza, 2013; Waite et al., 2008). Fluids that are released at large depths, due, for example, to metamorphic reactions and magma degassing, are bound to rise through intricate pathways and involve transient viscous drag forces and pressure gradients.

3. Fluid Flow in Permeable Fault Zones

Seismic activity is highly sensitive to the presence of fluids in fault zones (Rice, 1992; Sibson, 1992b; Sleep & Blanpied, 1994). The basic principle is that fluid pressure acts to lower the fault strength by decreasing the effective normal stress and reducing the threshold value of shear stress required for slippage. Accordingly, intermittent seismic activity may be due to fluctuations of fluid pressure. Mechanisms that have been proposed include shear-induced compaction in sealed fault segments leading to high pore pressure (Sleep & Blanpied, 1992) and the influx of high-pressure fluid from below the fault (Rice, 1992).

In contrast to upper crustal environments which involve mostly meteoric water, subduction zones are fed by fluids generated by dehydration metamorphic reactions at large depths and pressures (e.g., van Keken

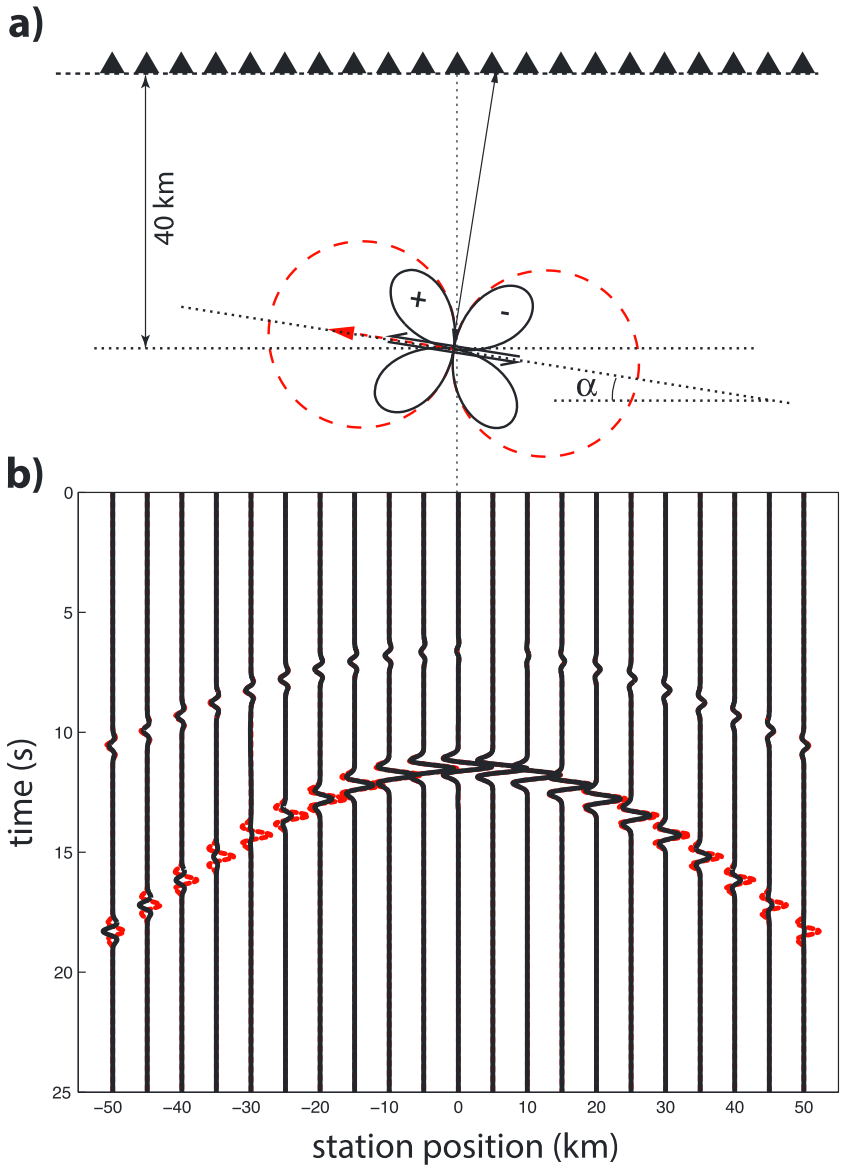


Figure 1. Comparison of radiation patterns from shear slip and single force seismic sources. (a) Schematic illustration of a source located at a 40 km depth recorded by seismic stations located at the surface. Normalized *P* wave radiation patterns for shear slip and single force sources are indicated with solid black and dashed red lines, respectively. (b) Synthetic seismograms computed in a homogeneous media (V_p = 6,062 m/s, V_s = 3,500 m/s) at stations shown in (a). Subduction dipping angle $\alpha = 7°$ has been considered. *P* waves from radial components were combined with *S* waves from transverse components. Waveforms were normalized by the *S* wave maximal amplitude at the nearest station.

et al., 2011). This difference of fluid supply has fundamental consequences for the magnitude of fluid pressure because the pervasive pathways connecting deep fluid sources to the surface may not exist and pressures are not constrained to remain close to hydrostatic values. In the deeper subduction zone environment, the most damaged and permeable zone is a thin channel along the subduction interface where metamorphic fluids are bound to rise (e.g., Angiboust et al., 2012, 2014, 2015). This is analogous to shallower fault zones where the strongly anisotropic permeability impedes fluid from moving in the perpendicular direction (e.g., Kawano et al., 2011; Kim et al., 2013; Mainprice et al., 2008). Geological studies (e.g., Saffer, 2015; Taetz et al., 2018) indicate that in fault zones, fluid flow is highly transient and limited to segments, resulting in relatively fast (i.e., occurring over a few months) pressure transients (e.g., Cruz-Atienza et al., 2018; Faulkner et al., 2018; Skarbek & Rempel, 2016) possibly associated with slow earthquakes (e.g., Frank et al., 2015; Toya et al., 2017). These observations imply that fault permeability varies by large amounts in both space and time.

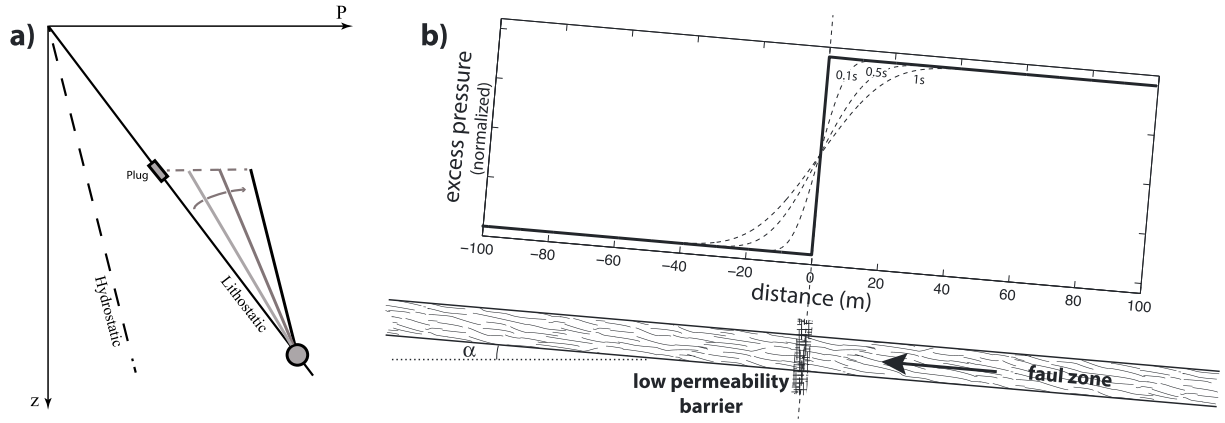


Figure 2. (a) Schematic illustration of the fluid pressure in a permeable zone of finite length between a source and an impermeable barrier. Fluid is generated at the source at the local lithostatic pressure and migrates upwards due to buoyancy. Due to flow, this initial phase is associated with a pressure gradient that exceeds the hydrostatic gradient. When the flow reaches the impermeable barrier, fluid flow slows down gradually and the pressure gradient decreases towards the hydrostatic value. Flow eventually stops, leading to a hydrostatic pressure gradient in the permeable zone and an elevated fluid pressure at the barrier. (b) Illustration of the conceptual locally fast fault-valve model predicting rapid fluid pressure variations in the subduction fault zone. The metamorphic fluid migrates updip along a permeable channel formed along the subduction interface. At position $x = 0$ is sealed by a barrier resulting in a pressure discontinuity, shown with the solid line. When the barrier is "broken" the fluid starts to migrate across the initial discontinuity. The resulting pressure evolution is described by equation (7). Pressure profiles predicted at 0.1s, 0.5s and 1 s after breaking the barrier with assuming $D = 10^2 m^2/s$ are shown with dashed lines.

3.1. Model Setup

Full and accurate modeling of a fluid flow along a 3-D heterogeneous plate interface or fault zone is a complex problem that is out of scope of our short paper. To perform the computations presented below, we adopt some significant simplifications. The first one is the 1-D approximation with considering a channel of constant width (Figure 2a) and with transport properties not changing across the channel. Based on geological results showing that in the vicinity of the brittle-to-ductile transition the plate interface contains thick layers of highly damaged rocks (e.g., Angiboust et al., 2015), the thickness of the channel can be between a few tens and a few hundreds of meters. In the next approximation, we consider that the absolute fluid movement speed is low, implying that the turbulent flow effects can be ignored. Such effects have been considered by Ghosh et al. (2010) to explain the very rapid migration of tectonic tremors. At the same time, these authors concluded that such regime requires long continuous conduits that are not likely to be present in the tremor-active regions. They suggested, that observed tremor migrations are rather related to the propagation of pressure pulses. We, therefore, consider a simple regime when diffusive pressure pulses can propagate along the plate interface and briefly discuss how the regimes with variable speeds of such pulses can emerge. In the end of this section, we present some additional arguments showing that the flow regime cannot be simply estimated from the apparent speeds of seismic migration. In a third approximation we strongly simplify the variations of the transport properties along the channel. Instead of considering continuous variations, we make the channel to be composed of segments with constant permeabilities and basically consider a binary distribution of the permeability: Long segments with a high "background" level of permeability are separated by low-permeability "barriers." The advantage of such simplification is that the solutions in each segment can be derived analytically.

The concept of "barrier" is central to our model. It represents small portions of the fault channel with locally very low permeability likely caused either by geometry (thinning) or by porosity reduction or by their combination. Fluid transport will result in building of strong pressure gradients across these barriers, as described in section 3.3. We than consider that when a barrier can be "broken" when the pressure difference rises above some threshold value. We assume that the mechanical breaking of the barrier is fast comparing to the timescale of the fluid flow and model it as an instantaneous increase of the permeability to the background channel level. After the breaking the accumulated overpressure is released and the barrier can become closed again. This idea is supported by geological observations (e.g., Angiboust et al., 2014; Fagereng et al., 2011) showing that the fault-zone rocks exhibit the breaking/healing cyclic behavior enhanced by fluid flux (e.g., Bernaudin & Gueydan, 2018). The barrier healing stage (not considered in our calculation) is governed by a combination of mechanical and chemical mechanisms. Extrapolation of results of the hot pressing

experiments (e.g., Giger et al., 2007) indicates that at the P-T conditions of the LFE source region the healing could occur on a few day time or faster scale.

In the following, after establishing basic equations governing pressure evolution in a 1-D homogeneous channel, we consider two simple cases. First, we consider "fast" pressure fluctuations associated with breaking barrier. Second, we show how the effective permeability of a fault channel is modified with respect to the numbers of open or closed barriers.

3.2. Fluid Pressure in a 1-D Porous Channel

Taking coordinate x in the up direction along a fault zone that dips at angle α, Darcy's law stipulates that the flow rate per unit area q is

$$q = \frac{\rho k}{\mu}\left[-\frac{\partial P}{\partial x} - \rho g \sin(\alpha)\right], \tag{1}$$

where ρ is the fluid density, k is permeability, μ is the fluid viscosity, and g is the acceleration of gravity. For a turbulent regime, head loss would involve a wall friction term proportional to u^2 (where u is the fluid motion speed) and hence to q^2. Regardless of the flow regime and permeability value, key principles are that flow only occurs when the fluid pressure gradient is larger than the hydrostatic value and that a hydrostatic fluid pressure gradient implies no flow. The total flux per unit breadth of the subduction zone is $Q = Aq$, where A is the channel cross-sectional area. Mass conservation dictates that

$$\frac{\partial(\rho\phi A)}{\partial t} = -\frac{\partial Q}{\partial x}, \tag{2}$$

where ϕ is porosity. One may easily show that pressure-induced changes of fluid density are small and do not modify significantly the body force term. Writing that porosity and fluid density vary with pressure and assuming that the top and base of the permeable zone do not deform significantly, which implies that section A does not vary with time, one obtains

$$\rho\phi\beta^* A\frac{\partial P}{\partial t} = \frac{\partial}{\partial x}\left(A\frac{\rho k}{\mu}\frac{\partial P}{\partial x}\right), \tag{3}$$

where β^* is an effective compressibility that accounts for both the fluid phase and the pore space. We shall be interested later in variations of permeability and/or channel cross-section along the subduction interface because they lead to a complex distribution of fluid pressure. If one neglects such variations, one obtains the familiar diffusion equation:

$$\frac{\partial P}{\partial t} = \frac{k}{\beta^*\phi\mu}\frac{\partial^2 P}{\partial x^2}, \tag{4}$$

where the hydraulic diffusivity is

$$D = \frac{k}{\beta^*\phi\mu}. \tag{5}$$

3.3. The Buildup of Fluid Pressure at a Barrier

We first consider an initially fluid-drained fault zone made of segments separated by zero porosity barriers spaced unevenly. At the end of a previous cycle, there is no continuous fluid phase in a segment and fluid may only be present in isolated small-scale pockets where fluid pressures are lithostatic. At the source (the base of the deepest segment), the fluid is released by deep metamorphic dehydration reactions in the subducting plate. The exact pressure conditions depend on the phase changes and induced density differences but, owing to the small fluid densities and weak density changes in dehydrating minerals, mass conservation implies that the local pressure is bound to exceed the ambient lithostatic value. A conservative estimate, therefore, is that fluid is released at the local lithostatic pressure, a condition that ensures that fluids gets expelled from its source and that existing fluid pathways do not get squeezed shut. The initial lithostatic fluid pressures allows an upward flow acting to develop connections between adjacent pockets. Once fluid has reached the impermeable barrier at the top of the segment, a continuous fluid phase has spread through the whole segment. At the top of the segment, the no throughflow condition implies that the local fluid pressure gradient is hydrostatic and that the local fluid pressure increases due to the incoming flow. Below the barrier, the flow rate decreases as the fluid pressure gradient gradually settles towards the hydrostatic value (Figure 2a). Eventually, if the barrier resists, flow stops as the fluid pressure gradient stabilizes at the hydrostatic value. Fluid-filled regions are at larger pressures than at the initial time (Figure 2a), which makes room

for the new fluid. For a barrier lying at distance l from the source, the total fluid pressure drop over that distance is equal to $\Delta P = \rho g \sin(\alpha) l$. Over the same distance, pressure decreases by $\Delta P_r = \rho_r g \sin(\alpha) l$ in encasing rocks. These two different pressure gradients imply that the fluid is overpressured, with a maximum at $x = l$:

$$\Delta P_m = \left(\rho_r - \rho\right) g l \sin(\alpha). \tag{6}$$

The updip side of the barrier lies at the base of another segment with a fluid at lithostatic pressures. A large fluid pressure drop has therefore built up across the barrier, which may ultimately cause its failure. Note however that equation (6) specifies the maximum fluid overpressure that can be achieved and that the barrier may break down for a smaller value depending on the material properties. Note also that the above arguments are valid for all flow regimes.

3.4. Pressure Changes and Displacements Induced by Barrier Failure

We use the diffusion equation (4) to describe the local evolution of fluid pressure when the barrier breaks down. The pressure profile across the barrier just before failure can be approximated by a step function as illustrated in Figure 2b. We consider that the barrier fails instantaneously. The solution of equation (4) with a pressure drop ΔP at $x = 0$ at $t = 0$ is given by

$$P(x,t) = \frac{\Delta P}{2} erf\left(\frac{x}{\sqrt{4Dt}}\right), \tag{7}$$

where *erf* stands for the error function and where $\Delta P \leq \Delta P_m$. A remarkable property of this solution is that the time dependance of the pressure propagation does not depend on ΔP and is only controlled by diffusivity D (equation (5)), implying that apparent duration of a corresponding seismic source does not depend on its magnitude.

The distributions of earthquakes in space and time within induced or naturally occurring seismic swarms have been used to estimate hydraulic diffusivity. Values in a 0.1- to 1.5-m^2/s range have been found for upper-crustal faults (e.g., Chen et al., 2012; Shapiro et al., 1997; Shelly et al., 2013). A similar approach has been applied to the source area of LFEs. For example, Frank et al. (2015) proposed that the spatial migration of LFE activity in Guerrero, Mexico, was due to pore-pressure propagation. Taking a porosity of 5% ($\phi = 0.05$), they inferred a fault zone permeability of $\approx 3 \cdot 10^{-12}$ m^2. For a fluid viscosity $\mu = 10^{-3}$ Pa s and compressibility $\beta^* = 2.2$ GPa^{-1}, $D \approx 10^2$ m^2/s. Interestingly, almost the same value of hydraulic diffusivity was inferred from the characteristics of long-period volcanic seismicity in the lower crust beneath Kamchatka volcanoes (Shapiro et al., 2017).

The evolution of the fluid pressure predicted by equation (7) with $D = 10^2$ m^2/s is shown in Figure 2b. As the barrier ruptures, fluid pressure propagates updip at a rate that is very high initially and decreases rapidly. Figure 3a shows how the fluid pressure changes at a distance of 5 m from the barrier. To approximately estimate the impact of such a pressure change on seismic radiation, we consider that the net force is applied to a 10-m-thick barrier. This force is obtained by multiplying the pressure from Figure 3a by the area of the permeable channel. The absolute value of the induced S wave surface displacement is (Aki & Richards, 2002)

$$u(t) = \frac{1}{4\pi\rho V_S^2 r} \Delta P A \left| P^{norm}(t) \right|, \tag{8}$$

where $P^{norm}(t)$ is the function shown in Figure 3a, V_S is the S wave speed and r is the distance between the failing barrier (i.e., the LFE source) and the recording seismometer. We use an over-pressure $\Delta P = 5$ MPa that, according to equation (6), can be built up over an approximately 300 m depth difference along the fault if the fluid density is close to that of water. The resulting displacement and velocity are shown in Figures 3b and 3c for $A = 10^3$ m^2, $V_S = 3.5$ km/s, $\rho = 2{,}850$ kg/m^3, and $r = 40$ km (a typical LFE depth). Figure 3d shows the velocity seismogram filtered between 1 and 8 Hz, a typical LFE frequency range. The predicted ground velocity is of the order of a few hundred nanometers per second, as observed for LFEs.

This simple model suggests that a seismogenic instability can be generated when an impermeable barrier breaks down, resulting in very fast pressure transients. The fluid flux decreases very rapidly and we can assume that, after some time, the barrier gets "healed" and that the sequence repeats itself. This results in a cyclic behavior controlled by the interplay of fluid flow and barrier breaching and healing. A very similar scenario known as the "fault-valve model" was proposed for the long-term intermittency of large earthquakes

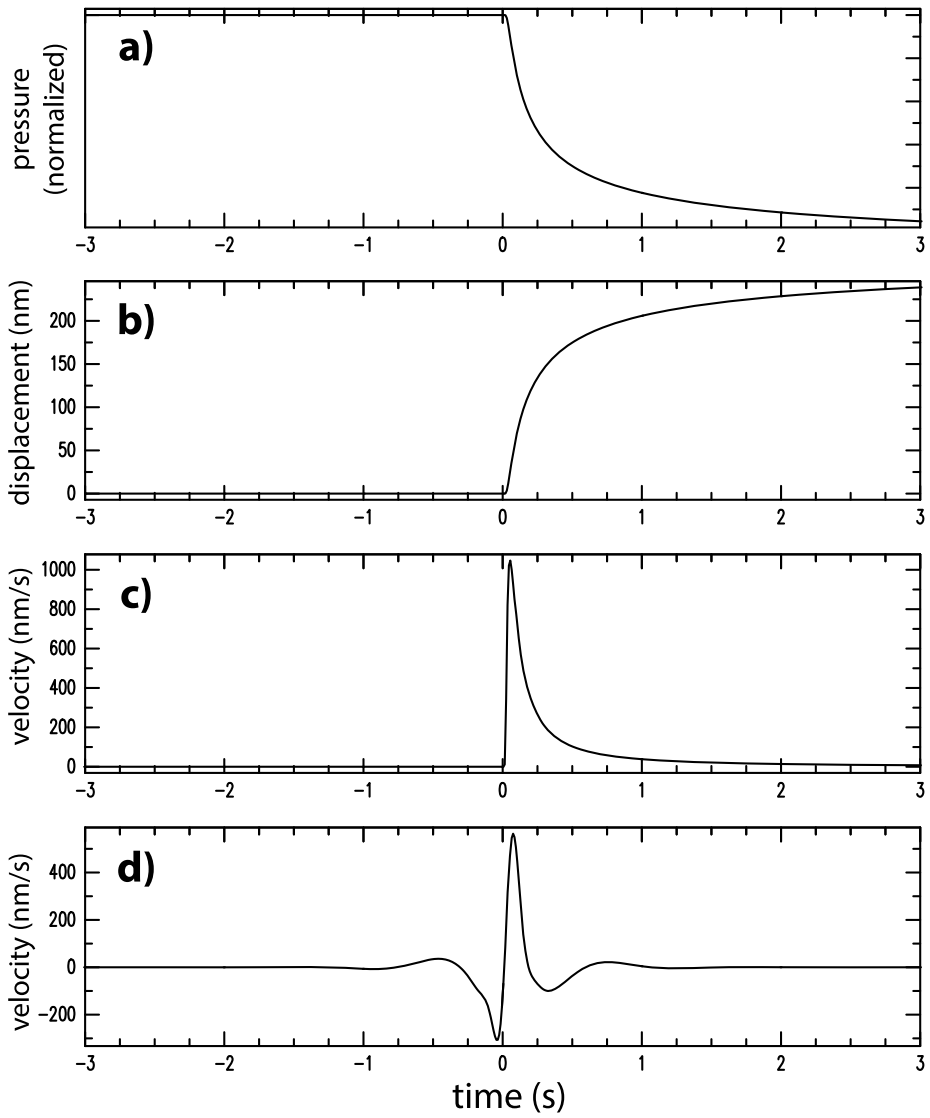


Figure 3. Evolution of fluid pressure and estimations of the ground motion predicted form the locally fast fault-valve model. (a) Pressure at $x = 0$. (b) *S* wave ground displacement at a location 40 km away from the source. (c) Corresponding ground velocity. (d) Velocity band-passed between 1 and 8 Hz.

(e.g., Sibson et al., 1988; Sibson, 1992a, 1992b). Here we propose that a similar cycle can occur in the LFE source area, albeit at much smaller space and time scales, corresponding to what can be called the "locally fast fault-valve model."

3.5. Fluid Pressure Distribution in a Channel With Low-Permeability Barriers

The previous model dealt with highly intermittent flow through a channel with a single barrier. We now consider a model involving a fluid-filled permeable channel with several low permeability barriers (Figure 4). In steady state, the bulk flow rate at any distance x from the source is

$$Q = constant = \rho \frac{Ak}{\mu} \left[-\frac{\partial P}{\partial x} - \rho g \sin(\alpha) \right]. \tag{9}$$

This is rewritten as follows:

$$\frac{\partial P}{\partial x} = -\frac{\mu}{\rho k A} Q - \rho g \sin(\alpha). \tag{10}$$

Thus, regions with smaller permeability and/or cross-sectional area are associated with pressure gradients that are much larger than average. The flow rate may be calculated as a function of the pressures at the two

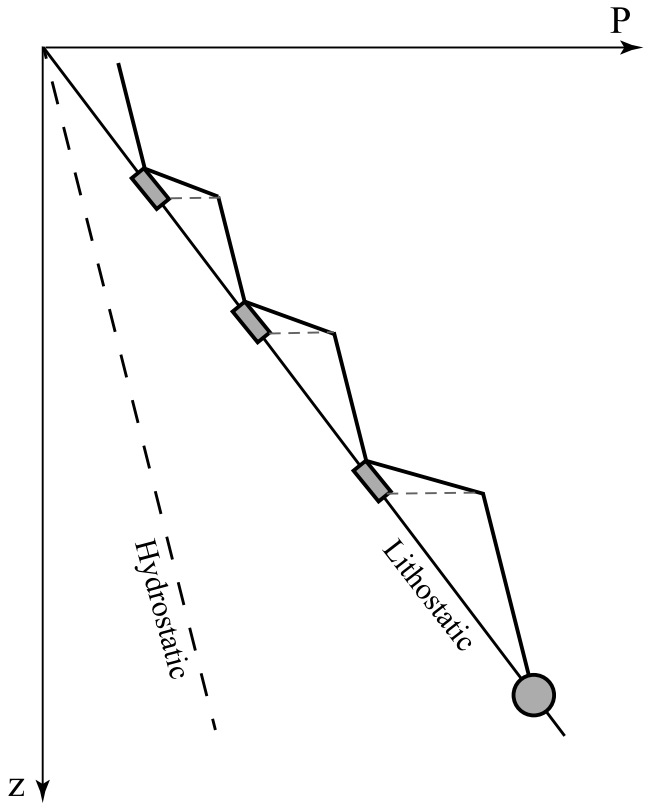


Figure 4. Schematic illustration of the distribution of fluid pressure in a fault zone with permeable segments separated by low permeability barriers. Steady state conditions are assumed, implying large values of the pressure gradient in the low permeability barriers and near-hydrostatic pressure gradients in the permeable segments. This system generates large pressure differences across the low permeability barriers.

ends of the channel. The values of these two pressures are irrelevant to our argument and can be adjusted to different configurations. At the deep end, we may assume lithostatic conditions as before. At the other end, two basic possibilities are lithostatic or hydrostatic pressures, with the latter corresponding to a patch that feeds a highly permeable accretionary wedge, for example. Denoting the pressure difference between the two ends of the channel by ΔP_L and integrating the previous equation over the channel length L, one obtains

$$\Delta P_L - \rho g \sin\alpha L = \Delta P_T = Q \int_0^L \frac{\mu}{\rho k A} \mathrm{d}x, \tag{11}$$

where ΔP_T is the driving pressure for the flow. Let us consider a series of N barriers with very small permeabilities. If N is sufficiently large the integral on the right-hand side is dominated by contributions from the barriers, such that

$$\Delta P_T \approx Q \frac{\mu}{\rho} \sum_{j=1}^{N} \frac{\Delta l_j}{k_j A_j}, \tag{12}$$

where Δl_j is the length of the j barrier.

For a constant-section channel and assuming that all barriers are identical, i.e., have the same permeability k_b and the same length Δl_b, equation (12) can be simplified with introducing an effective permeability k^{eff} for a channel of total length L:

$$k^{eff} \approx \frac{k_b L}{N \Delta l_b}. \tag{13}$$

Equations (12) and (13) show that the effective permeability of a "heterogeneous fault channel" depends on the number of closed versus open barriers. The overall increase of the fluid flux and pressure gradient will facilitate the opening of the barriers, that is, the occurrence of the LFE, and will result in an overall increase of the fault permeability. Such system is prone to emergence of pore-pressure waves with variable speeds (e.g., Cruz-Atienza et al., 2018; Rice, 1992) that can explain the different migration patterns and clustering of LFE and tremors (e.g., Frank et al., 2016; Ghosh et al., 2010).

An important consequence is that the flow regime is not dictated by the permeable patches, but by the barriers. In a steady state (not including the transients following barrier failures), the fluid flow q is constant. Based on the equivalent channel model for permeability (Paterson, 1983) q can be expressed as

$$q = \rho a^2 u \phi \tag{14}$$

and related to the local Reynolds number

$$Re = \frac{\rho u a}{\mu} \tag{15}$$

as

$$Re = \frac{q}{\mu} \frac{1}{a\phi}, \tag{16}$$

where ρ is the fluid density, μ is the fluid viscosity, u is a representative fluid velocity, ϕ is the porosity, and a the typical width of the fluid pathways. This shows that Re is proportional to quantity $(1/a\phi)$, which is largest in the low permeability barriers due to both their narrower than average pathways and lower than average porosity. Thus, the flow regime cannot be ascertained from the apparent permeability value, which is much larger than that of the barriers (equation (13)).

4. LFE Activity and Fluid Release From Dehydrating Slabs

For a seismic source governed by the fast fault-valve model, we can estimate the corresponding volume of fluid migrating across the barrier $\Delta V(t)$ from the pressure change and the fluid (water) compressibility β:

$$\Delta V(t) = \phi\beta A \int_0^\infty \left(\frac{\Delta P}{2} - P(x,t)\right) \mathrm{d}x, \tag{17}$$

where $P(x,t)$ is predicted by equation (7). As shown in Figure 3, the rate of pressure change decreases to very small values a few seconds after barrier failure. We thus set the LFE duration at ~ 3 s. Using this time and parameter values from previous sections ($\phi = 0.05, \delta P = 5$ MPa, $D = 10^2$ m^2/s), the volume of fluid transported across a barrier during one LFE event is $\Delta V^{LFE} \approx 1$ m^3.

Let us assume that all LFEs are generated by the same mechanism. LFEs do not conform to power-law distributions and have the same characteristic amplitude (e.g., Aso et al., 2013; Chamberlain et al., 2014; Frank et al., 2014). We may therefore estimate the total fluid volume involved as follows:

$$V^{LFE} = \frac{N^{LFE}\,\Delta V^{LFE}}{N}, \tag{18}$$

where N^{LFE} is the total number of LFE and N is the average number of barriers that fluid encounters as it flows updip along the subduction interface. Frank et al. (2014) detected $\sim 2 \cdot 10^6$ LFEs in 2.5 years in Guerrero, Mexico. From our estimate of ΔV^{LFE}, this LFE activity requires $V^{LFE} \leq 760,000$ m^3/year.

This estimate can be compared to the amount of fluids that are generated by slab dehydration. Using dehydration rates calculated by van Keken et al. (2011) for a large range of subduction conditions, we estimate that the young Cocos plate releases ~ 10 Tg Myr^{-1} m^{-1} in the top 70 km of the Mexico subduction zone. This can be re-calculated as 10 m^3 of water per year per unit slab breadth. The breadth of the LFE generating zone in the Guerrero area is ~ 50 km resulting in $V^{subd} \approx 500{,}000$ m^3/year. If we assume that the migrating fluids break down more than two "barriers," this fluid flux is able to account for the observed LFE activity.

5. Discussion and Conclusions

Fluid transport and shearing of the fault zone may be strongly coupled (e.g., Phipps Morgan & Holtzman, 2005). "Barriers" are associated with irregularities of the subduction interface, which determine the strength of the fault. Individual breakdown events are not necessarily associated with slippage but act to reduce the interface roughness, which effectively reduces the fault strength and may ultimately be responsible for shear motion. LFEs may be regarded as due to short pore-pressure pulses coupled to larger and slower shear deformation in the form of a very low frequency earthquake (e.g., Ando et al., 2012; Ghosh et al., 2015; Ide, 2016; Ito et al., 2007). Overall, a full description of the mechanisms generating seismic waves during slow earthquakes is likely to require models where shear deformation and fluid transport processes are dynamically coupled.

A final point concerns the interface roughness, which evolves on two different time-scales. On the time-scale of a seismic sequence, barrier breakdown facilitates slippage but slippage does not rid the fault zone of barriers. On the contrary, shear displacement acts to create new areas of low permeability through two mechanisms. Shear deformation of the fault zone material leads to an intrinsic permeability decrease through grain crushing, pore collapse, and increasing tortuosity, in other words due to damage processes (Lyakhovsky & Hamiel, 2007; Zhu & Wong, 1996; Zhu et al., 1997). At the scale of the channel thickness, the relative shear displacement of the two rough bounding surfaces acts to decrease the bulk permeability in the displacement direction and to enhance it in the perpendicular direction (Auradou et al., 2005; Yeo et al., 1998). Interestingly, these changes are due in large part to the occurrence of large ridges perpendicular to the displacement direction (Auradou et al., 2005), which may well be the barriers of our model. On a longer time scale, subduction zone fluids are highly charged and reactive aqueous solutions bound to enhance roughness by dissolution/precipitation processes.

It is now recognized that fault zone fluids play a major role in the physics of slow earthquakes (e.g., Audet et al., 2009; Frank et al., 2015; Kim et al., 2010; Song et al., 2009; Toya et al., 2017). These fluids have been mostly considered as "passive" with only an impact on effective pressure, but may well play an active role. We have argued that rapid changes of flow conditions can result in fast "dynamic" seismogenic pressure variations. In our simple conceptual model, seismic sources are generated by the failure of barriers in permeable fault zones. The large pressure drop that builds up across a barrier gets relaxed rapidly and imparts a large impulsive force able to generate seismic displacements with LFE characteristics (including amplitudes and radiation patterns). Dehydration reactions in subducting plates release amounts of fluids that are large enough to sustain LFE activity.

The LFE have also been observed in large strike slip faults (e.g., Nadeau & Dolenc, 2005). Analysis of radiation patterns in such settings in beyond the scope of our paper. We just note here that high pore pressure fluids supplied from the mantle or deep crust have been suggested to play important role in the generation of tectonic tremors in the San Andreas fault (e.g., Becken et al., 2011; Thomas et al., 2009).

A fluid-related source mechanism accounts for several other LFE features. It naturally predicts that the duration of an LFE event does not depend on magnitude (e.g., Bostock et al., 2015; Farge et al., 2017). Duration is controlled by hydraulic diffusivity D whilst magnitude depends on the accumulated fluid pressure, which depends in turn on the material strength. This mechanism is therefore consistent with the narrow range of LFE magnitudes (e.g., Aso et al., 2013; Chamberlain et al., 2014; Frank et al., 2014). In addition, the propagation of fluid pressure in channel with variable permeability can provide mechanisms for different observed migration patterns and clustering of LFE and tremors (e.g., Ghosh et al., 2010; Frank et al., 2016).

Acknowledgments
This study was supported by the Russian Ministry of Education and Science (grant N 14.W03.31.0033) and by the European Research Council under the European Union Horizon 2020 research and innovation program (grant agreement 742335 - F-IMAGE). There are no new data in the paper.

References

Aki, K., & Richards, P. G. (2002). *Quantitative seismology*. Sausalito, CA: University Science Books. Retrieved from https://books.google.fr/books?id=sRhawFG5_EcC

Ando, M., Tu, Y., Kumagai, H., Yamanaka, Y., & Lin, C.-H. (2012). Very low frequency earthquakes along the Ryukyu subduction zone. *Geophysical Research Letters*, *39*, L04303. https://doi.org/10.1029/2011GL050559

Angiboust, S., Kirsch, J., Oncken, O., Glodny, J., Monié, P., & Rybacki, E. (2015). Probing the transition between seismically coupled and decoupled segments along an ancient subduction interface. *Geochemistry, Geophysics, Geosystems*, *16*, 1905–1922. https://doi.org/10.1002/2015GC005776

Angiboust, S., Pettke, T., De Hoog, J. C. M., Caron, B., & Oncken, O. (2014). Channelized fluid flow and eclogite-facies metasomatism along the subduction shear zone. *Journal of Petrology*, *55*(5), 883–916. https://doi.org/10.1093/petrology/egu010

Angiboust, S., Wolf, S., Burov, E., Agard, P., & Yamato, P. (2012). Effect of fluid circulation on subduction interface tectonic processes: Insights from thermo-mechanical numerical modelling. *Earth and Planetary Science Letters*, *357-358*, 238–248.

Aso, N., Ohta, K., & Ide, S. (2013). Tectonic, volcanic, and semi-volcanic deep low-frequency earthquakes in western japan. *Tectonophysics*, *600*, 27–40. http://https://doi.org/10.1016/j.tecto.2012.12.015, Great Earthquakes along Subduction Zones.

Audet, P., Bostock, M. G., Christensen, N. I., & Peacock, S. M. (2009). Seismic evidence for overpressured subducted oceanic crust and megathrust fault sealing. *Nature*, *457*, 76–78. https://doi.org/10.1038/nature07650

Auradou, H., Drazer, G., Hulin, J. P., & Koplik, J. (2005). Permeability anisotropy induced by the shear displacement of rough fracture walls. *Water Resources Research*, *41*, W09423. https://doi.org/10.1029/2005WR003938

Becken, M., Ritter, O., Bedrosian, P. A., & Weckmann, U. (2011). Correlation between deep fluids, tremor and creep along the central san andreas fault. *Nature*, *480*, 87–90. https://doi.org/10.1038/nature10609

Bernaudin, M., & Gueydan, F. (2018). Episodic tremor and slip explained by fluid-enhanced microfracturing and sealing. *Geophysical Research Letters*, *45*, 3471–3480. https://doi.org/10.1029/2018GL077586

Bostock, M. G., Royer, A. A., Hearn, E. H., & Peacock, S. M. (2012). Low frequency earthquakes below southern Vancouver island. *Geochemistry, Geophysics, Geosystems*, *13*, Q11007. https://doi.org/10.1029/2012GC004391

Bostock, M. G., Thomas, A. M., Savard, G., Chuang, L., & Rubin, A. M. (2015). Magnitudes and moment-duration scaling of low-frequency earthquakes beneath southern Vancouver island. *Journal of Geophysical Research: Solid Earth*, *120*, 6329–6350. https://doi.org/10.1002/2015JB012195

Chamberlain, C. J., Shelly, D. R., Townend, J., & Stern, T. A. (2014). Low-frequency earthquakes reveal punctuated slow slip on the deep extent of the Alpine fault, New Zealand. *Geochemistry, Geophysics, Geosystems*, *15*, 2984–2999. https://doi.org/10.1002/2014GC005436

Chen, X., Shearer, P. M., & Abercrombie, R. E. (2012). Spatial migration of earthquakes within seismic clusters in southern California: Evidence for fluid diffusion. *Journal of Geophysical Research*, *117*, B04301. https://doi.org/10.1029/2011JB008973

Chouet, B. A. (1996). Long-period volcano seismicity: Its source and use in eruption forecasting. *Nature*, *380*, 309–316. https://doi.org/10.1038/380309a0

Chouet, B. A., & Matoza, R. S. (2013). A multi-decadal view of seismic methods for detecting precursors of magma movement and eruption. *Journal of Volcanology and Geothermal Research*, *252*, 108–175. https://doi.org/10.1016/j.jvolgeores.2012.11.013

Cruz-Atienza, V. M., Villafuerte, C., & Bhat, H. S. (2018). Rapid tremor migration and pore-pressure waves in subduction zones. *Nature Communications*, *9*(1), 2900. https://doi.org/10.1038/s41467-018-05150-3

Dahlen, F. A. (1993). Single-force representation of shallow landslide sources. *Bulletin of the Seismological Society of America*, *83*(1), 130–143.

Ekström, G., Nettles, M., & Abers, G. A. (2003). Glacial earthquakes. *Science*, *302*(5645), 622–624. https://doi.org/10.1126/science.1088057

Fagereng, A., Remitti, F., & Sibson, R. H. (2011). Incrementally developed slickenfibers—Geological record of repeating low stress-drop seismic events? *Tectonophysics*, *510*(3), 381–386. https://doi.org/10.1016/j.tecto.2011.08.015

Farge, G., Shapiro, N. M., Frank, W. B., Mercury, N., Vilotte, J.-P., & KISS working group (2017). Insights in low frequency earthquake source processes from observations of their size-duration scaling. In *American Geophysical Union, Fall Meeting 2017*, Abstract S53-F03. New Orleans.

Faulkner, D. R., Sanchez-Roa, C., Boulton, C., & den Hartog, S. A. M. (2018). Pore fluid pressure development in compacting fault gouge in theory, experiments, and nature. *Journal of Geophysical Research: Solid Earth*, *123*, 226–241. https://doi.org/10.1002/2017JB015130

Favreau, P., Mangeney, A., Lucas, A., Crosta, G., & Bouchut, F. (2010). Numerical modeling of landquakes. *Geophysical Research Letters*, *37*, L15305. https://doi.org/10.1029/2010GL043512

Fehler, M. (1983). Observations of volcanic tremor at Mount St. Helens Volcano. *Journal of Geophysical Research*, *88*(B4), 3476–3484. https://doi.org/10.1029/JB088iB04p03476

Frank, W. B., Shapiro, N. M., Husker, A. L., Kostoglodov, V., Bhat, H. S., & Campillo, M. (2015). Along-fault pore-pressure evolution during a slow-slip event in Guerrero, Mexico. *Earth and Planetary Science Letters*, *413*, 135–143. https://doi.org/10.1016/j.epsl.2014.12.051

Frank, W. B., Shapiro, N. M., Husker, A. L., Kostoglodov, V., Gusev, A. A., & Campillo, M. (2016). The evolving interaction of low-frequency earthquakes during transient slip. *Science Advances*, *2*(4), e1501616. https://doi.org/10.1126/sciadv.1501616

Frank, W. B., Shapiro, N. M., Husker, A. L., Kostoglodov, V., Romanenko, A., & Campillo, M. (2014). Using systematically characterized low-frequency earthquakes as a fault probe in Guerrero, Mexico. *Journal of Geophysical Research: Solid Earth*, *119*, 7686–7700. https://doi.org/10.1002/2014JB011457

Frank, W. B., Shapiro, N. M., Kostoglodov, V., Husker, A. L., Campillo, M., Payero, J. S., & Prieto, G. A. (2013). Low-frequency earthquakes in the Mexican sweet spot. *Geophysical Research Letters*, *40*, 2661–2666. https://doi.org/10.1002/grl.50561

Ghosh, A., Huesca-Pérez, E., Brodsky, E., & Ito, Y. (2015). Very low frequency earthquakes in Cascadia migrate with tremor. *Geophysical Research Letters*, *42*, 3228–3232. https://doi.org/10.1002/2015GL063286

Ghosh, A., Vidale, J. E., Sweet, J. R., Creager, K. C., Wech, A. G., Houston, H., & Brodsky, E. E. (2010). Rapid, continuous streaking of tremor in Cascadia. *Geochemistry, Geophysics, Geosystems*, *11*, Q12010. https://doi.org/10.1029/2010GC003305

Giger, S. B., Tenthorey, E., Cox, S. F., & Fitz Gerald, J. D. (2007). Permeability evolution in quartz fault gouges under hydrothermal conditions. *Journal of Geophysical Research*, *112*, B07202. https://doi.org/10.1029/2006JB004828

Husker, A. L., Kostoglodov, V., Cruz-Atienza, V. M., Legrand, D., Shapiro, N. M., Payero, J. S., et al. (2012). Temporal variations of non-volcanic tremor (NVT) locations in the mexican subduction zone: Finding the NVT sweet spot. *Geochemistry, Geophysics, Geosystems*, *13*, Q03011. https://doi.org/10.1029/2011GC003916

Ide, S. (2016). Characteristics of slow earthquakes in the very low frequency band: Application to the Cascadia subduction zone. *Journal of Geophysical Research: Solid Earth*, *121*, 5942–5952. https://doi.org/10.1002/2016JB013085

Ide, S., Shelly, D. R., & Beroza, G. C. (2007). Mechanism of deep low frequency earthquakes: Further evidence that deep non-volcanic tremor is generated by shear slip on the plate interface. *Geophysical Research Letters*, *34*, L03308. https://doi.org/10.1029/2006GL028890

Imanishi, K., Uchide, T., & Takeda, N. (2016). Determination of focal mechanisms of nonvolcanic tremor using S wave polarization data corrected for the effects of anisotropy. *Geophysical Research Letters*, *43*, 611–619. https://doi.org/10.1002/2015GL067249

Ito, Y., Obara, K., Shiomi, K., Sekine, S., & Hirose, H. (2007). Slow earthquakes coincident with episodic tremors and slow slip events. *Science*, *315*(5811), 503–506. https://doi.org/10.1126/science.1134454

Kanamori, H., & Given, J. W. (1982). Analysis of long-period seismic waves excited by the May 18, 1980, eruption of Mount St. Helens—A terrestrial monopole? *Journal of Geophysical Research*, *87*(B7), 5422–5432. https://doi.org/10.1029/JB087iB07p05422

Kanamori, H., Given, J. W., & Lay, T. (1984). Analysis of seismic body waves excited by the mount st. helens eruption of may 18, 1980. *Journal of Geophysical Research*, *89*(B3), 1856–1866. https://doi.org/10.1029/JB089iB03p01856

Kao, H., Shan, S.-J., Dragert, H., Rogers, G., Cassidy, J. F., & Ramachandran, K. (2005). A wide depth distribution of seismic tremors along the northern Cascadia margin. *Nature*, *436*, 841–844. http://doi.org/10.1038/nature03903

Kawakatsu, H. (1989). Centroid single force inversion of seismic waves generated by landslides. *Journal of Geophysical Research*, *94*(B9), 12,363–12,374. https://doi.org/10.1029/JB094iB09p12363

Kawano, S., Katayama, I., & Okazaki, K. (2011). Permeability anisotropy of serpentinite and fluid pathways in a subduction zone. *Geology*, *39*(10), 939–942. https://doi.org/10.1130/G32173.1

Kim, Y. H., Clayton, R. W., Asimow, P. D., & Jackson, J. M. (2013). Generation of talc in the mantle wedge and its role in subduction dynamics in central Mexico. *Earth and Planetary Science Letters*, *384*, 81–87. https://doi.org/10.1016/j.epsl.2013.10.006

Kim, Y., Clayton, R. W., & Jackson, J. M. (2010). Geometry and seismic properties of the subducting cocos plate in central mexico. *Journal of Geophysical Research*, *115*, B06310. https://doi.org/10.1029/2009JB006942

Kostoglodov, V., Husker, A., Shapiro, N. M., Payero, J. S., Campillo, M., Cotte, N., & Clayton, R. (2010). The 2006 slow slip event and nonvolcanic tremor in the mexican subduction zone. *Geophysical Research Letters*, *37*, L24301. https://doi.org/10.1029/2010GL045424

Lyakhovsky, V., & Hamiel, Y. (2007). Damage evolution and fluid flow in poroelastic rock. *Izvestiya, Physics of the Solid Earth*, *43*(1), 13–23.

Mainprice, D., Page, Y. L., Rodgers, J., & Jouanna, P. (2008). Ab initio elastic properties of talc from 0 to 12 GPa: Interpretation of seismic velocities at mantle pressures and prediction of auxetic behaviour at low pressure. *Earth and Planetary Science Letters*, *274*(3), 327–338.

Nadeau, R. M., & Dolenc, D. (2005). Nonvolcanic tremors deep beneath the san andreas fault. *Science*, *307*(5708), 389–389. https://doi.org/10.1126/science.1107142

Obara, K. (2002). Nonvolcanic deep tremor associated with subduction in southwest Japan. *Science*, *296*(5573), 1679–1681. http://doi.org/10.1126/science.1070378

Obara, K., & Hirose, H. (2006). Non-volcanic deep low-frequency tremors accompanying slow slips in the southwest Japan subduction zone. *Tectonophysics*, *417*(1), 33–51. https://doi.org/10.1016/j.tecto.2005.04.013

Paterson, M. S. (1983). The equivalent channel model for permeability and resistivity in fluid-saturated rock—A re-appraisal. *Mechanics of Materials*, *2*(4), 345–352. https://doi.org/10.1016/0167-6636(83)90025-X

Payero, J. S., Kostoglodov, V., Shapiro, N., Mikumo, T., Iglesias, A., Pérez-Campos, X., & Clayton, R. W. (2008). Nonvolcanic tremor observed in the mexican subduction zone. *Geophysical Research Letters*, *35*, L07305. https://doi.org/10.1029/2007GL032877

Phipps Morgan, J., & Holtzman, B. K. (2005). Vug waves: A mechanism for coupled rock deformation and fluid migration. *Geochemistry, Geophysics, Geosystems*, *6*, Q08002. https://doi.org/10.1029/2004GC000818

Rice, J. R. (1992). Fault stress states, pore pressure distributions, and the weakness of the San Andreas fault. In B. Evans, & T.-f Wong (Eds.), *Fault mechanics and transport properties of rocks, International geophysics* (Vol. 51, pp. 475–503). San Diego, CA: Academic Press.

Rogers, G., & Dragert, H. (2003). Episodic tremor and slip on the Cascadia subduction zone: The chatter of silent slip. *Science*, *300*(5627), 1942–1943. https://doi.org/10.1126/science.1084783

Royer, A. A., & Bostock, M. G. (2014). A comparative study of low frequency earthquake templates in northern Cascadia. *Earth and Planetary Science Letters*, *402*, 247–256. https://doi.org/10.1016/j.epsl.2013.08.040, Special issue on USArray science.

Saffer, D. M. (2015). The permeability of active subduction plate boundary faults. *Geofluids*, *15*(1-2), 193–215.

Schwartz, S. Y., & Rokosky, J. M. (2007). Slow slip events and seismic tremor at circum-pacific subduction zones. *Reviews of Geophysics*, *45*, RG3004. https://doi.org/10.1029/2006RG000208

Shapiro, N. M., Droznin, D. V., Droznina, S. Y., Senyukov, S. L., Gusev, A. A., & Gordeev, E. I. (2017). Deep and shallow long-period volcanic seismicity linked by fluid-pressure transfer. *Nature Geoscience*, *10*, 442–445. https://doi.org/10.1038/ngeo2952

Shapiro, S. A., Huenges, E., & Borm, G. (1997). Estimating the crust permeability from fluid-injection-induced seismic emission at the KTB site. *Geophysical Journal International*, *131*(2), F15–F18. https://doi.org/10.1111/j.1365-246X.1997.tb01215.x

Shelly, D. R., Beroza, G. C., & Ide, S. (2007). Non-volcanic tremor and low-frequency earthquake swarms. *Nature*, *446*, 305–307. https://doi.org/10.1038/nature05666

Shelly, D. R., Beroza, G. C., Ide, S., & Nakamula, S. (2006). Low-frequency earthquakes in Shikoku, Japan, and their relationship to episodic tremor and slip. *Nature*, *442*, 188–191. https://doi.org/10.1038/nature04931

Shelly, D. R., Hill, D. P., Massin, F., Farrell, J., Smith, R. B., & Taira, T. (2013). A fluid-driven earthquake swarm on the margin of the yellowstone caldera. *Journal of Geophysical Research: Solid Earth*, *118*, 4872–4886. https://doi.org/10.1002/jgrb.50362

Sibson, R. H. (1992a). Implications of fault-valve behaviour for rupture nucleation and recurrence. *Tectonophysics*, *211*(1), 283–293. https://doi.org/10.1016/00401951(92)90065-E

Sibson, R. H. (1992b). Fault-valve behavior and the hydrostatic-lithostatic fluid pressure interface. *Earth-Science Reviews*, *32*(1), 141–144. https://doi.org/10.1016/00128252(92)90019-P

Sibson, R. H., Robert, F., & Poulsen, K. H. (1988). High-angle reverse faults, fluid-pressure cycling, and mesothermal gold-quartz deposits. *Geology*, *16*(6), 551–555. https://doi.org/10.1130/0091-7613(1988)016<0551:HARFFP>2.3.CO;2

Skarbek, R. M., & Rempel, A. W. (2016). Dehydration-induced porosity waves and episodic tremor and slip. *Geochemistry, Geophysics, Geosystems*, *17*, 442–469. https://doi.org/10.1002/2015GC006155

Sleep, N. H., & Blanpied, M. L. (1992). Creep, compaction and the weak rheology of major faults. *Nature*, *359*, 687–689. https://doi.org/10.1038/359687a0

Sleep, N. H., & Blanpied, M. L. (1994). Ductile creep and compaction: A mechanism for transiently increasing fluid pressure in mostly sealed fault zones. *Pure and Applied Geophysics*, *143*(1), 9–40. https://doi.org/10.1007/BF00874322

Song, T.-R. A., Helmberger, D. V., Brudzinski, M. R., Clayton, R. W., Davis, P., Pérez-Campos, X., & Singh, S. K. (2009). Subducting slab ultra-slow velocity layer coincident with silent earthquakes in southern mexico. *Science*, *324*(5926), 502–506. https://doi.org/10.1126/science.1167595

Taetz, S., John, T., Bröcker, M., Spandler, C., & Stracke, A. (2018). Fast intraslab fluid-flow events linked to pulses of high pore fluid pressure at the subducted plate interface. *Earth and Planetary Science Letters*, *482*, 33–43. https://doi.org/10.1016/j.epsl.2017.10.044

Takei, Y., & Kumazawa, M. (1994). Why have the single force and torque been excluded from seismic source models? *Geophysical Journal International*, *118*(1), 20–30. https://doi.org/10.1111/j.1365-246X.1994.tb04672.x

Thomas, A. M., Nadeau, R. M., & Bürgmann, R. (2009). Tremor-tide correlations and near-lithostatic pore pressure on the deep San Andreas fault. *Nature*, *462*, 1048–1051. https://doi.org/10.1038/nature08654

Toya, M., Kato, A., Maeda, T., Obara, K., Takeda, T., & Yamaoka, K. (2017). Down-dip variations in a subducting low-velocity zone linked to episodic tremor and slip: A new constraint from SCSP waves. *Scientific Reports*, *7*(1), 2868. https://doi.org/10.1038/s41598-017-03048-6

van Keken, P. E., Hacker, B. R., Syracuse, E. M., & Abers, G. A. (2011). Subduction factory: 4. depth-dependent flux of H_2O from subducting slabs worldwide. *Journal of Geophysical Research*, *116*, B01401. https://doi.org/10.1029/2010JB007922

Waite, G. P., Chouet, B. A., & Dawson, P. B. (2008). Eruption dynamics at Mount St. Helens imaged from broadband seismic waveforms: Interaction of the shallow magmatic and hydrothermal systems. *Journal of Geophysical Research*, *113*, B02305. https://doi.org/10.1029/2007JB005259

Walter, J. I., Schwartz, S. Y., Protti, J. M., & Gonzalez, V. (2011). Persistent tremor within the northern Costa Rica seismogenic zone. *Geophysical Research Letters*, *38*, L01307. https://doi.org/10.1029/2010GL045586

Wech, A. G., & Creager, K. C. (2007). Cascadia tremor polarization evidence for plate interface slip. *Geophysical Research Letters*, *34*, L22306. https://doi.org/10.1029/2007GL031167

Yeo, I. W., de Freitas, M. H., & Zimmerman, R. W. (1998). Effect of shear displacement on the aperture and permeability of a rock fracture. *International Journal of Rock Mechanics and Mining Sciences*, *35*(8), 1051–1070. https://doi.org/10.1016/S01489062(98)00165-X

Zhu, W., Montesi, L. G. J., & Wong, T.-f. (1997). Shear-enhanced compaction and permeability reduction: Triaxial extension tests on porous sandstone. *Mechanics of Materials*, *25*(3), 199–214.

Zhu, W., & Wong, T.-F. (1996). Permeability reduction in a dilating rock: Network modeling of damage and tortuosity. *Geophysical Research Letters*, *23*(22), 3099–3102.